Strong-field-induced bond rearrangement in triatomic molecules

S. Zhao,[1] Bethany Jochim,[2] Peyman Feizollah,[2] Jyoti Rajput,[2,*] F. Ziaee,[2] Kanaka Raju P.,[2] B. Kaderiya,[2] K. Borne,[2] Y. Malakar,[2] Ben Berry,[2] J. Harrington,[2] D. Rolles,[2] A. Rudenko,[2] K. D. Carnes,[2] E. Wells,[1,†] I. Ben-Itzhak,[2,‡] and T. Severt[2,§]

[1]*Department of Physics, Augustana University, Sioux Falls, South Dakota 57197, USA*

[2]*J. R. Macdonald Laboratory, Physics Department, Kansas State University, Manhattan, Kansas 66506, USA*

A comparative study of bond rearrangement is reported for the double ionization of three triatomic molecules: carbon dioxide, carbonyl sulfide, and water (D_2O). Specifically, we study the formation of the molecular cation AC^+ from the edge atoms of a triatomic molecular dication ABC^{2+} following double ionization by intense, short (23 fs, 790 nm) laser pulses. The comparison is made using the double ionization branching ratio of each molecule, thereby minimizing differences due to differing ionization rates. The rearrangement branching ratio is highest for water, which has a bent initial geometry, while CO_2 and OCS are linear molecules. The angular distribution of $O_2{}^+$ fragments arising from CO_2 is essentially isotropic, while SO^+ from OCS and $D_2{}^+$ from D_2O are aligned with the laser polarization. In the CO_2 and D_2O cases, the angular distributions of the bond rearrangement channels are different from the angular distributions of the dominant dissociative double ionization channels $CO^+ + O^+$ and $OD^+ + D^+$. Only the angular distribution of SO^+ from OCS is both aligned with the laser polarization and similar to the angular distribution of the largest dissociative channel, $CO^+ + S^+$. The mixed behavior observed from the angular distributions of the different molecules stands in contrast to the relative consistency of the magnitude of the bond rearrangement branching ratio.

I. INTRODUCTION

The breaking and subsequent formation of new molecular bonds in unimolecular chemical reactions has attracted considerable attention in recent years [1–30]. Examples of such processes include roaming [4,10,13,17,19,24], in which a neutral moiety traverses the molecule to capture another atom, hydrogen migration [9,12,15,16,18,20,21,25], and bond rearrangement [1,3,5–8,11,14,22,23,28,30], in which the cleaving of multiple bonds initiates a process leading to the formation of a new molecule from atoms that were not previously bonded to each other. A number of prominent photochemical reactions involve these processes, including decomposition of water [31] or NO_3 [32,33] by photolysis, the conversion of carbon dioxide to oxygen in the atmosphere [26,34], the combustion of hydrocarbons [12,15,20,25], and the formation of $H_3{}^+$ from alcohols [10,24]. In addition, there is expanding interest in moving beyond observing the dynamics of these processes to controlling those dynamics using ultrafast lasers (see, for example, Refs. [20,35,36]).

Despite the increasing attention devoted to these processes, so far most studies focused on a single molecular species and occurred under an assortment of experimental conditions. For example, the initiating ionization mechanism in previous bond rearrangement studies has variously included single [8,11,37–42] and multiple photons [5,22,26,27,43] as well as electron [23,28,44] and heavy ion impact [2,7,30]. To assist in understanding these dynamics we examine bond rearrangement following ultrafast strong-field double ionization of three triatomic molecules: carbon dioxide, carbonyl sulfide, and water. It is hoped that this comparative study will provide baseline data that drives theoretical explorations of these processes.

To make a more meaningful cross-molecule comparison, we consider bond rearrangement in the context of the double-ionization branching ratio for each molecule, that is, the ratio of the bond rearrangement yield to the total yield of all the one-, two-, and three-body breakup channels following double ionization. This method of comparison [29,45–49] minimizes the effect of the different ionization potentials across the molecules since the different ionization potentials naturally lead to different rates of double ionization at the same laser intensity. To accurately obtain this ratio, all of the nonnegligible dissociative and nondissociative channels resulting from the ABC^{2+} parent must be evaluated.

As illustrated in Fig. 1, the three target molecules have different characteristics. CO_2 is linear and mass symmetric, OCS is linear but mass asymmetric, and water is bent and has a different highest occupied molecular orbital (HOMO) configuration than either CO_2 or OCS. The three neutral molecules have different ground-state vibrational frequencies for both stretching and bending modes (see Table I), and certainly have different vibrational frequencies for the associated molecular ions. A cross-molecule comparison can begin to probe how some of these factors might influence the bond rearrangement process. Since we perform an ion-ion coincidence measurement using a cold-target-recoil-ion-momentum-spectroscopy

———————

*Present address: Department of Physics and Astrophysics, University of Delhi, Delhi 110007, India.

†eric.wells@augie.edu

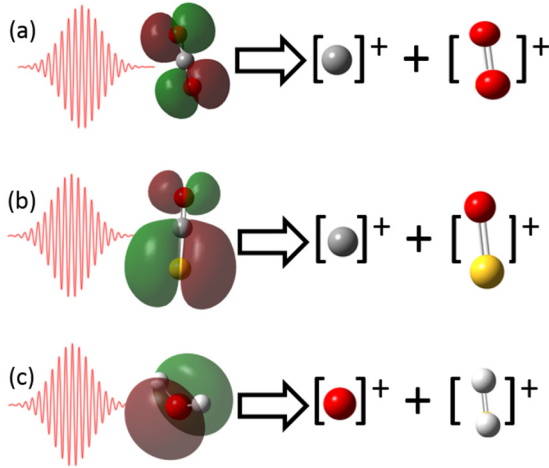‡ibi@phys.ksu.edu

§tsevert@phys.ksu.edu

FIG. 1. The three molecules studied in this experiment along with the associated bond rearrangement channel. The HOMO of each target molecule is shown. (a) $CO_2 + n\omega \rightarrow O_2^+ + C^+$. (b) OCS $+ n\omega \rightarrow SO^+ + C^+$. (c) $D_2O + n\omega \rightarrow D_2^+ + O^+$.

(COLTRIMS) [50,51] method, the data not only contain yields of the channels needed to calculate the branching ratio, but also the momentum vectors of the dissociating molecular fragments. From this three-dimensional data we evaluate the angular distributions and kinetic energy release (KER) distributions of the bond rearrangement process in the different molecules and also comment on previous strong-field measurements of bond rearrangements in CO_2 [26,27] and water [5,22,43,52].

Sections II and III describe the experimental method and data analysis procedures, respectively, that allow the accurate evaluation of the branching ratios in these targets despite the small overall magnitude of the bond rearrangement channel (around 0.1% order of magnitude in all cases) compared to other double-ionization channels. In Sec. IV we discuss overall trends in the branching ratio and some details of the measurements of each individual target. Our experiment indicates that the bond rearrangement branching ratio is highest in the water target. The difference in the bond rearrangement branching ratio between the three molecules is less than an order of magnitude.

II. EXPERIMENTAL METHOD

The laser pulses in this experiment have 23 fs (FWHM in intensity) pulse duration, a central wavelength of 790 nm, and

TABLE I. Vibrational frequencies for the stretching and bending modes of neutral CO_2, D_2O, and OCS. Values are from NIST [53].

Molecule	Symmetric Stretch cm^{-1}		Bend cm^{-1}
CO_2	1333		667
D_2O	2671		1178
	CO stretch cm^{-1}	CS stretch cm^{-1}	Bend cm^{-1}
OCS	2062	859	520

TABLE II. Bond rearrangement branching ratios following double ionization of CO_2, OCS, and D_2O. R includes all the channels listed in Tables III to V.

Molecular dissociation	Intensity $(10^{14}\ W/cm^2)$	R (%)
$CO_2^{2+} \rightarrow O_2^+ + C^+$	7.2 ± 1.3	0.0796 ± 0.0058
$OCS^{2+} \rightarrow SO^+ + C^+$	5.6 ± 0.8	0.0253 ± 0.0014
$D_2O^{2+} \rightarrow D_2^+ + O^+$	6.6 ± 1.0	0.199 ± 0.016

maximum pulse energy of 2 mJ. These pulses are produced at a 10-kHz repetition rate by a KMLabs ultrafast Ti:Sapphire chirped-pulse-amplification laser system known as PULSAR [54]. The laser pulse is characterized using second-harmonic-generation frequency-resolved-optical-gating (SHG-FROG) [55]. The peak laser intensity is determined by measuring the recoil momentum distribution of Ne^+ ions along the laser polarization and locating the point associated with the $2U_p$ kinetic energy of the electron [56], where U_p is the ponder-motive energy. At this point, rescattered electrons become more dominant than direct electrons in the above-threshold-ionization photoelectron spectrum. Intensities in these experiments were between 5.6 and $7.2 \times 10^{14}\ W/cm^2$ as specified in Table II.

An $f = 7.5$ cm spherical mirror is used to focus the laser beam onto the supersonic molecular beam of a COLTRIMS [50,51] apparatus, from which all the charged products from the triatomic target are measured in coincidence by a time- and position-sensitive detector. The OCS gas was seeded into a helium buffer gas to cool the target and control the total count rate on the detector. On the other hand, the CO_2 and D_2O targets were not seeded in any buffer gas. The target molecules are randomly oriented with respect to the laser polarization in the supersonic molecular beam. The base pressure in the spectrometer region was below 2×10^{-10} Torr, and the count rate on the detector was around 15 kHz, or approximately 1.5 ions per laser pulse. Since the charged fragments are recorded on an event-by-event basis, we can use momentum conservation in conjunction with the measured time and position of all the charged fragments to reconstruct the three-dimensional momentum distributions, as will be described below.

III. DATA ANALYSIS

In coincident molecular fragmentation studies, a standard way to describe the likelihood of a particular outcome is with a branching ratio [29,45–49,57,58]. (The branching ratio is sometimes called the "relative cross-section," "abundance," or "fragmentation pattern.") We compute the branching ratio by dividing the yield of a specific coincidence channel by the sum of all possible products originating from a specific transient molecular ion such as ABC^{2+}. The branching ratio for bond rearrangement of a doubly charged triatomic molecule, i.e., ABC^{2+} going to $AC^+ + B^+$, is

$$R = \frac{M(AC^+ + B^+)}{\varepsilon \sum_i M(^{(1)}P_i) + \sum_j M(^{(2)}P_j) + \sum_k M(^{(3)}P_k)}, \quad (1)$$

where M stands for the measured counts in each channel after subtracting false coincidences (described below), $^{(1)}P$
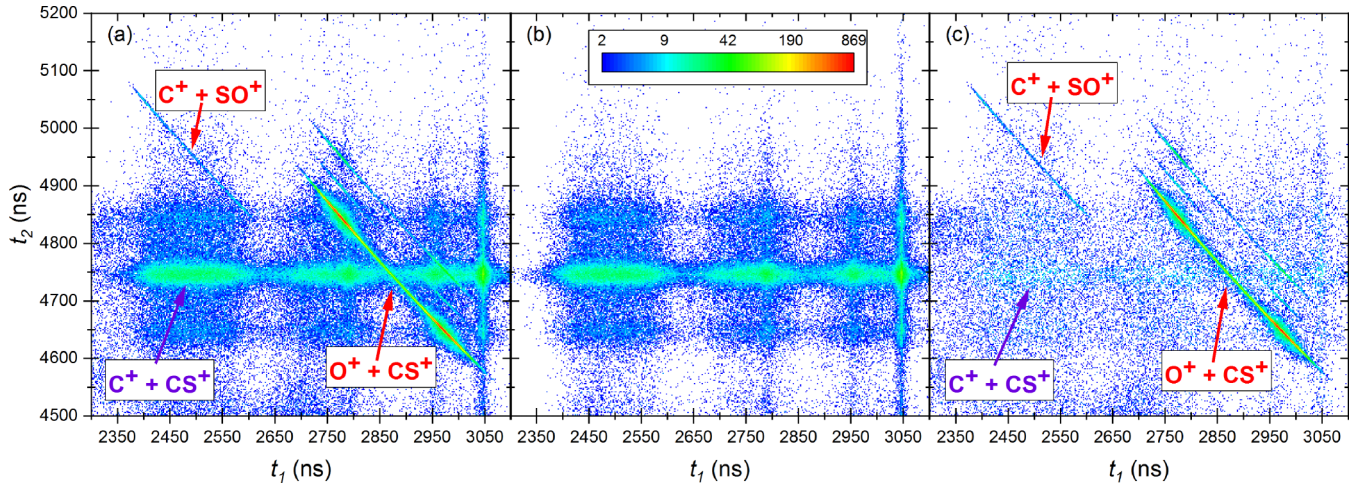
FIG. 2. A region of the CTOF data for the OCS measurement. (a) Measured data with the diagonal two-body breakup islands visible for several channels, including $C^+ + SO^+$ at the upper left. This bond rearrangement channel is clearly visible without any correction. An example false coincidence channel, $C^+ + CS^+$, is indicated with the purple arrow and text. (b) Simulated false coincidence spectrum. (c) The CTOF yield after subtraction of the scaled simulated false coincidence spectrum. Two-body breakup channels are identified. The main $^{(12)}C^{32}S^+ + O^+$ channel is accompanied by smaller satellite channels due to naturally occurring $^{(13)}C$, $^{(33)}S$, and $^{(34)}S$ isotopes. These channels are too small to be visible in the $C^+ + SO^+$ bond rearrangement channel.

denotes all channels with a final dicationic charge state where only single dication products were measured (including channels such as ABC^{2+}, $AB^{2+} + C$, and $A^{2+} + BC$), $^{(2)}P$ stands for all the two-body ion pair breakup channels (i.e., $AB^+ + C^+$, $B^+ + AC^+$, and $C^+ + AB^+$) and $^{(3)}P$ stands for all the three-body fragmentation channels where only the ion pairs are measured in coincidence (like $A^+ + B^+ + C$, $A^+ + B + C^+$ and $A + B^+ + C^+$). Note that the $^{(1)}P$ channels are multiplied by the detection efficiency, ε, to correct for the difference in detection efficiency of single ions (ε) with respect to ion pairs (ε^2), where we assumed the same detection efficiency for all ions.

The advantage of calculating the branching ratio with respect to all possible channels of the doubly ionized parent, as in Eq. (1), rather than the total yield of all measured ions is that when making a cross-molecule comparison, effects due to target dependent factors, such as the ionization potential, are minimized [29]. If, however, the population of the daughter dication changes with intensity, that can modify the branching ratio and make cross-molecule comparisons more complicated.

The goal of the data analysis is the extraction of the yields of the various $^{(1)}P$, $^{(2)}P$, and $^{(3)}P$ channels that are needed to calculate R. There are some complications to be addressed in this process: One factor is that due to nonuniform detection efficiency across the surface of the detector, we correct the yield for position-dependent losses on our detector using known symmetries about the laser polarization. Additional complicating factors we address are the presence of false coincidences, which affect the yields of $^{(2)}P$ and $^{(3)}P$, and the detection efficiency, which is needed to properly scale the $^{(1)}P$ yields and to subtract the contributions of higher charge states which affect the $^{(3)}P$ yield. The following paragraphs summarize how we address these points.

Since we are operating in the regime of ~ 1 ion per laser pulse, we have a significant contribution from false coinci-

dences, that is, coincident ions that arise from the fragmentation of two or more molecules in the same laser pulse. To reduce their effect on the calculated branching ratio, we generate the false coincident ion pairs by randomly pairing ions from different laser pulses [2,59–61]. Since we can generate an arbitrary number of random ion pairs, we identify a purely random feature in any spectrum and generate enough false coincidences to match it, so it is properly subtracted. For example, in Fig. 2 we show how to subtract randoms in the coincidence time-of-flight (CTOF) map for OCS. In particular, Fig. 2(a) shows the $SO^+ + C^+$ and $CS^+ + O^+$ channels, which appear as narrow diagonal stripes typical of two-body (i.e., momentum conserving) breakup of the parent molecule [62,63]. In addition, we also observe false coincidence structures, such as the $C^+ + CS^+$ false coincidence peak indicated by the purple arrow in Fig. 2(a). We scale the false coincidence distribution, shown in Fig. 2(b), to this purely random feature and subtract them to produce the "random free" spectrum shown in Fig. 2(c).

To analyze the two-body double-ionization breakup channels [$^{(2)}P$ contributions], we calculate the momenta of each fragment in the center-of-mass frame of the breakup (see, for example, Ref. [64]). To limit the contributions of other channels and other possible sources of contamination, we set gates on the laboratory frame momentum sum, i.e., the momentum distribution of the center of mass of the parent molecule.

To analyze the three-body breakup channels associated with double ionization [$^{(3)}P$ contributions], we select the apparent ion-pair coincidence channels containing an undetected third atomic fragment. Due to the high intensities of these measurements, the missing atom can either be neutral or charged. When the missing fragment is charged, we measure the complete three-body channel, scale it by the detection efficiency, and subtract it to reveal the three-body coincidence channel with a missing neutral fragment. To determine the

detection efficiency, we choose a three-body ion-pair coincidence channel where the features of channels due to a third missing neutral and charged fragment are clearly separated. The detection efficiency is then the scaling factor required to subtract the contributions associated with the missing charged fragment. For an example using a similar method for determining the detection efficiency using only two-body breakup, see Ref. [65]. Then, to calculate the momentum of the missing atom, we compute the initial laboratory-frame velocities of the measured ionic fragments and subtract the average initial center-of-mass velocity of the parent molecule, as determined from the coincidence channels where all fragments are measured. Using momentum conservation, we compute the momentum of the neutral atom.

Since momentum conservation is used to determine the momentum of the neutral fragment, it cannot also be used to compute the initial spread in the center-of-mass momentum due to the temperature of the molecular beam. Therefore, the momentum resolution is worse than the case of breakup channels where all fragments are measured. Fortunately, the increased uncertainty is minimal because the initial spread of the center-of-mass momentum, i.e., the temperature of the molecular beam, is low. For example, in the OCS measurement, the transverse temperature of the molecular beam was $\sim 6\,\mathrm{K}$ while the longitudinal temperature was $\sim 125\,\mathrm{K}$. The temperatures were determined by examining the sum of momentum distributions in the laboratory frame. When determining the yield of each three-body channel with a neutral fragment, we correct for the competing isotopically substituted channels that cannot be separated using the isotopic abundance of each atom from the NIST database [66].

In analyzing the three-body channels, we neglect most charge asymmetric channels from the dication, like O^{2+} + C + S in OCS, which are expected to have a lower rate than the charge symmetric channels [67,68]. The present OCS data supports this assumption, showing CS^{2+} + O is less than 0.2% of the total double ionization yield, about an order of magnitude less than the smallest of the three-body channels containing two singly charged and one neutral fragment, $C^+ + O^+ + S$. Since we are mainly interested in the branching ratio of the bond rearrangement channels, the effect of the charge asymmetric channels is minimal because their yields only contribute to the denominator of Eq. (1).

Aside from statistical uncertainties, the primary contributions to the uncertainty in the evaluated branching ratio are due to the random coincidence subtraction and the corrections for position dependent losses.

IV. RESULTS AND DISCUSSION

The main result of this experiment is the branching ratio of the bond rearrangement channels from double ionization of CO_2, OCS, and D_2O. These findings are summarized in Table II. There are two immediate conclusions that can be drawn from the results. First, bond rearrangement is more likely in D_2O than in CO_2, which in turn is more likely than bond rearrangement in OCS. Second, all of the R values are within an order of magnitude.

Carbon dioxide has been described as a "showcase" [40] for the complexities involved in molecular fragmentation pro-

cesses. The intricacies in the fragmentation and isomerization of CO_2 can depend on the charge state of the ion [69–74], metastable states of the dication [75–78], the Renner-Teller effect [40,71], and the geometry of excited states [71,79]. As a result of these interesting features, CO_2 fragmentation has been examined using electron [77,80–83] and ion impact [84–86] as well as various photoionization studies [40,41,69–74,87,88].

Several of these studies noted the production of O_2^+ fragments [26,27,40,41], although we are not aware of any reports of the branching ratio. The results of our double ionization branching ratio measurement for CO_2 are reported in Table III.

Two recent strong-field studies of CO_2 report the observation of the $CO_2 + n\omega \rightarrow O_2^+ + C^+$ process induced with laser pulses centered near 800 nm [26,27]. While neither of these experiments reports an explicit branching ratio, Larimian *et al.* do point out that the yield of $O_2^+ + C^+$ is approximately three orders of magnitude lower than the $CO^+ + O^+$ channel [26]. Their estimate is consistent with our result, which was at nearly identical pulse duration but somewhat higher intensity: $(7.2 \pm 1.3) \times 10^{14}\,\mathrm{W/cm^2}$ in our measurement compared to $10^{14}\,\mathrm{W/cm^2}$ in their measurement [26].

There have been a number of previous studies of the fragmentation dynamics in OCS following strong-field multiple ionization [42,89–93], as well as similar studies using single photon [8,90,94–98], ion [99,100], and electron impact [101]. Many of these studies examined three-body breakup and did not focus on the bond rearrangement channel leading to SO^+ formation. Our results for the double ionization branching ratio in OCS are shown in Table IV. The strong preference for

TABLE III. Branching ratios of the measured final products of doubly ionized CO_2 at $(7.2 \pm 1.3) \times 10^{14}\,\mathrm{W/cm^2}$. The $CO^+ + O^+$ channel contains contributions from both "prompt" and "dissociation in flight," as discussed in the text.

Fragmentation Channel	R (%)
$CO^+ + O^+$	65.6 ± 4.5
$C^+ + O^+ + O$	23.7 ± 7.3
CO_2^{2+}	6.08 ± 0.81
$O^+ + O^+ + C$	4.6 ± 1.4
$C^+ + O_2^+$	0.0796 ± 0.0058

TABLE IV. Branching ratios of the measured final products of doubly ionized OCS at $(5.6 \pm 0.8) \times 10^{14}\,\mathrm{W/cm^2}$.

Fragmentation channel	R (%)
OCS^{2+}	63.4 ± 6.2
$CO^+ + S^+$	26.8 ± 1.4
$C^+ + S^+ + O$	5.2 ± 1.3
$O^+ + S^+ + C$	1.55 ± 0.40
$C^+ + O^+ + S$	1.49 ± 0.38
$CS^+ + O^+$	1.358 ± 0.072
$CS^{2+} + O$	0.159 ± 0.015
$SO^+ + C^+$	0.0253 ± 0.0014

TABLE V. Branching ratios of the measured final products of doubly ionized D_2O at $(6.6 \pm 1.0) \times 10^{14}\,\mathrm{W/cm^2}$. As noted in the text, the absence of the D_2O^{2+} channel is expected from the details of the potential energy surface of the ground electronic state of D_2O^{2+}.

Fragmentation channel	R (%)
$D^+ + DO^+$	74.6 ± 5.0
$D^+ + O^+ + D$	22.1 ± 6.8
$D^+ + D^+ + O$	3.10 ± 0.95
$D_2^+ + O^+$	0.199 ± 0.016

$CO^+ + S^+$ over $CS^+ + O^+$ has been ascribed to the fact that the C-O bond is stronger than the C-S bond in OCS^{2+} [39,97]. Here we note that the two-body $CS^+ + O^+$ channel is even smaller than the three-body channels. We are not aware of any previous measurements of the double ionization branching ratio that include the $SO^+ + C^+$ channel.

Bond rearrangement in water has been the subject of a variety of studies using ion [30,102,103] and electron [44] impact as well as single [11,37,38,42] and multiple photon absorption [5,22,43,52]. Oxygen core excitation via synchrotron radiation [11,37,38,42] suggests that the stimulation of bending motion, or a combination of bending and symmetric stretch modes, enhances the production of H_2^+. The process leading to the formation of H_2^+ is thought to be rapid in these situations, as short as 10 fs on the dication surface [11,42]. While fast ion impact predominantly interacts with valence, rather than core, electrons, the bond rearrangement process appears to be explained by a rapid process in these cases as well, specifically a vertical ionization to the dication leading to a small probability of reaching the $H_2^+ + O^+$ dissociation limit [2,30,44].

When water is ionized by very short laser pulses (5–10 fs), bond rearrangement has been reported to occur in several measurements [5,22,43]. Recent measurements by McCracken *et al.* [52], in contrast, reported no evidence of bond rearrangement in D_2O when ionized by 40-fs, 800-nm pulses. We observe $D_2O^{2+} \rightarrow D_2^+ + O^+$ bond rearrangement at a pulse duration of 23 fs, in between the shorter [5,22] and longer [52] pulses used in earlier experiments. As reported in Table II, R for water is larger than for CO_2 or OCS. The detailed analysis of the D_2O fragmentation, presented in Table V, shows that there is no yield in the main $^{(1)}P$ channel (i.e., D_2O^{2+}). This is expected because the potential well of the ground electronic state of the water dication is shallow, supporting states with lifetime around 1 ps or smaller [104]. In addition, there may be small amounts of contamination in the $D^+ + D^+ + O$ and $D^+ + O^+ + D$ channels. We estimate that the contamination should have a negligible effect on the branching ratio of $D_2^+ + O^+$, which is the main channel of interest.

A theme throughout previous studies of bond rearrangement [8,11,14,22,23,26–28,39–42] has been that the primary initiating step is the stimulation of bending modes in the triatomic molecule. With this background, it is not surprising that the bent water molecule has the highest bond rearrangement branching ratio of the molecules examined in this study. In addition to the favorable configuration of the neutral target,

the lighter mass of the deuterium atoms in D_2O can lead to larger vibrational amplitude than for oxygen or sulfur in CO_2 and OCS, respectively, meaning that a vertical projection of the neutral vibrational wave function onto the dication potential energy surface(s) will sample extensive parts of the surface(s), leading to the possibility of a greater range of dissociation outcomes. This qualitative argument can also explain why SO^+ is less likely to form from OCS than O_2^+ is from CO_2, since the sulfur atom is double the oxygen mass. Similar isotopic trends were observed in studies of bond rearrangement in methane, ammonia and water [7,30].

The above discussion assumes a vertical transition from the neutral to the dication potential energy surface. Note, however, that since we are studying bond rearrangement in a strong laser field, it is possible for the double ionization to occur in two steps. Specifically, once the molecule is singly ionized, the wave packet can evolve on the cation potential energy surfaces for a short time within the duration of the laser pulse before the molecule is further ionized, a dominant mechanism in many dissociative ionization cases (see, e.g., the review by Codling and Frasinski [105]). However, the relative importance of this mechanism in bond rearrangement is an open question because of the need for significant change in the nuclear geometry during the laser pulse. Such a "two-step" ionization mechanism was invoked by Larimian *et al.* [26] for O_2^+ formation from CO_2, which is described in more detail later in this article. Even during stepwise ionization, however, the wave packets associated with lighter fragments can evolve more rapidly on the cation surfaces, allowing more favorable bond rearrangement geometries to be reached before the laser pulse initiates the second ionization step. Since our measurement cannot distinguish direct versus stepwise double ionization, we can not exclude either possibility. To explore the role of intermediate cationic states, it may help to perform Fourier transform vibrational spectroscopy measurements using a strong-field femtosecond pump-probe scheme [26,106,107].

In addition, while the simple vertical ionization explanation above describes the trends in the branching ratio across the molecules, a comparison of the angular distributions of the bond rearrangement channels gives indications of more complex dynamics. Figures 3 and 4 show the angular distributions of the bond rearrangement channels in OCS and D_2O, respectively. In both of these molecules, the bond rearrangement fragment tends to be ejected along the laser polarization direction. Several previous studies [22,39,43] described particular mechanisms, specific to each molecule, that explain this aligned dissociation.

As a heteronuclear, nonsymmetric, linear, polar molecule, OCS has been a standard molecule for studies of alignment-dependent ionization, e.g., Refs. [108–111]. Double ionization of OCS leading to OCS^{2+} at $2 \times 10^{14}\,\mathrm{W/cm^2}$ is minimized for $\cos\theta = \pm 1$ [111], although the main two-body dissociative $CO^+ + S^+$ channel is peaked at $\cos\theta = \pm 1$. Both the dissociative and nondissociative distributions are thought to become less sharply peaked as the laser intensity increases and more dication states are accessible [111]. Our observation, shown in Fig. 3, is that the bond rearrangement ($SO^+ + C^+$) angular distribution follows the same trend as the main dissociative double ionization channel ($CO^+ + S^+$).
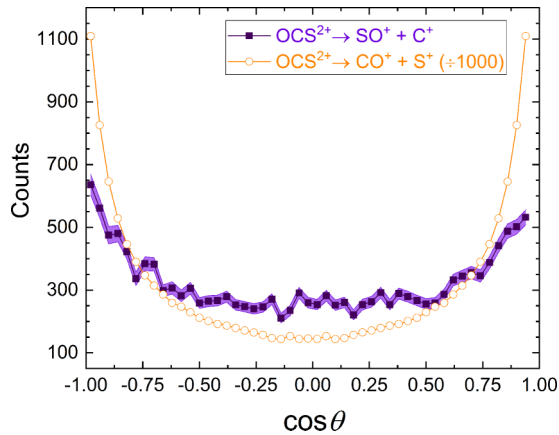
FIG. 3. The angular distribution of the $OCS^{2+} \rightarrow SO^+ + O^+$ bond rearrangement channel (solid purple squares) and the main two-body fragmentation channel $OCS^{2+} \rightarrow CO^+ + S^+$ (open orange circles). Here θ is the angle between the laser polarization and the direction of the lighter fragment of the ion-pair. The shaded regions indicate the uncertainty in the measurements and are small for the $OCS^{2+} \rightarrow CO^+ + S^+$ channel.

FIG. 5. The angular distribution of the $CO_2^{2+} \rightarrow O_2^+ + C^+$ (solid blue circles) and $CO_2^{2+} \rightarrow CO^+ + O^+$ (open red squares) where θ is the angle between the laser polarization and the direction of the lighter dissociating fragment in each ion-pair. The shaded regions indicate the uncertainty in the measurements. The dips near $\cos\theta = \pm 1$ are due to reduced detection efficiency near the center of the detector.

While the ground-state configuration of the neutral OCS molecule is linear, the minimum energy configuration of the dication is bent [112], with an energetic barrier of about 4 eV separating the linear and nonlinear configurations. Brites *et al.* [39] performed calculations that show that at an OCS angle of about 150°, the OCS^{2+} undergoes isomerization from OCS^{2+} to CSO^{2+}. In other words, in this process the oxygen atom migrates to the other side of the molecule. Brites *et al.* further predicted that the lowest electronic state of the CSO^{2+} isomer is repulsive, leading to dissociation into $C^+ + SO^+$ reaction products, as observed by Sorensen *et al.* [8,42]. This process increases when driven by resonant excitation of the $C\,1s \rightarrow \pi^*$ transition that induces a bending mode which is
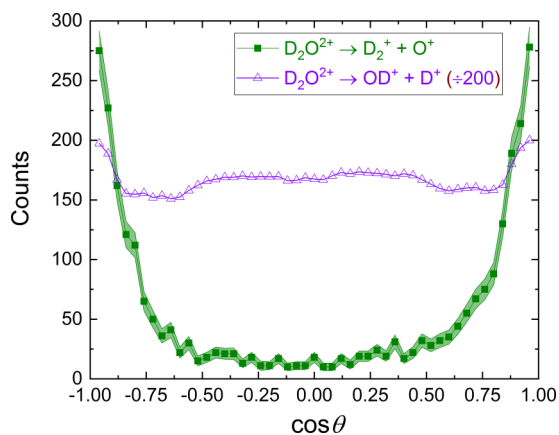

FIG. 4. The angular distribution of the $D_2O^{2+} \rightarrow D_2^+ + O^+$ (filled green squares) and $D_2O^{2+} \rightarrow OD^+ + D^+$ (open violet triangles) channels where θ is the angle between the laser polarization and the direction of the least massive fragment in the respective ion-pair. The shaded regions indicate the uncertainty in the measurements. The small decrease in the $OD^+ + D^+$ distribution around $\cos\theta = 0$ is likely due to a small fraction of D^+ fragments missing the detector.

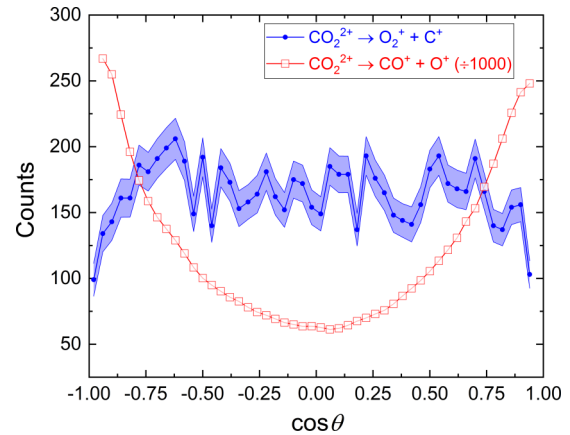further enhanced by the Renner-Teller effect [8]. This mechanism is triggered if the photoabsorption induces a bending mode with the transition dipole aligned with the polarization direction [8].

If inducing a bending mode that eventually leads to isomerization reaching a dissociative CSO^{2+} state is also the primary driver of $SO^+ + C^+$ production in strong-field ionization (the previous work [8,39,42,112] involved single photons), then one would expect a similar alignment when the process is initiated with a linearly polarized laser pulse. Indeed, our measured angular distribution is peaked along the polarization direction, similar to the single photon data [8]. The peak of our measured KER distribution is located at approximately 5.5 eV, 1.5 eV higher than the value predicted by Brites *et al.* [39] for dissociation of the lowest electronic state of the CSO^{2+} into $SO^+ + C^+$, showing that there are differences between the single-photon and strong-field measurements despite the similarities of the fragment angular distributions. Additional theoretical efforts are needed to develop further insight into the strong-field dynamics.

Like the OCS results, our measured $D_2^+ + O^+$ angular distribution, shown in Fig. 4, is peaked along the laser polarization direction. In contrast, the main $OD^+ + D^+$ fragmentation channel has a much less aligned distribution. Thus we conclude that the angular distribution of the bond rearrangement channels is not generally the same as the predominant double-ionization channel. Mathur *et al.* [22] examined the dynamics of the bond rearrangement process using velocity map imaging after ionization by 10-fs, 790-nm laser pulses. Our measured angular distributions, shown in Fig. 4, are consistent with the shorter pulse measurement [22], with both showing that $D_2^+ + O^+$ fragment ejection is strongly peaked along the laser polarization.

While the OCS and D_2O bond rearrangement channels are aligned along the laser polarization, the angular distribution for $CO_2^{2+} \rightarrow O_2^+ + C^+$ shown in Fig. 5 is isotropic, at least within the uncertainty of our measurement. The angular

distribution of the bond rearrangement channels is also different than the angular distribution of the dominant double ionization channel, $CO_2^{2+} \rightarrow CO^+ + O^+$, which, as shown in Fig. 5, is strongly peaked along the laser polarization direction. These differences can originate from the angular dependence of the ionization process. Previous measurements of single- and double-ionization of CO_2 have shown that the ionization is peaked for different angles between the laser polarization and the molecular axis depending on the final state of the (di)cation [106,113,114]. For example, $CO_2^{2+} \rightarrow CO^+ + O^+$ is peaked for ionization parallel to the polarization [106], while the ionization is peaked perpendicular and at $45°$ to the polarization for other final states [106,113,114]. If a number of these CO_2^{2+} states lead to bond rearrangement, then the resulting angular distribution from the combination could be approximately isotropic.

Another possible explanation of the isotropic angular distribution for $CO_2^{2+} \rightarrow O_2^+ + C^+$ shown in Fig. 5 are the dynamics of the bond rearrangement process. Based on their COLTRIMS measurements, associated calculations and further pump-probe measurements, Larimian *et al.* [26] hypothesized that O_2^+ formation occurs after the nuclear wave packet evolves on the CO_2^+ potential energy surface toward a bent configuration, which they estimate to occur within 25 fs. In their model, subsequent ionization to a CO_2^{2+} surface with a triangular configuration initiates the ejection of the carbon atom.

One possible explanation of the isotropic angular distribution for the $O_2^+ + C^+$ bond rearrangement channel is that there is a delay, after the rapid formation of the triangular dicationic CO_2^{2+} states within the laser pulse duration, that "erases" any angular dependence of the initial step(s) in the bond rearrangement process. If this is the case, the lifetime of the dication would need to be longer than the rotational period of CO_2^{2+} but shorter than ~ 150 ns. Longer lifetimes would be detected as dissociation in flight (see, for example Ref. [115]). The lower limit set by the rotational period is ≈ 33 ps for the $J = 1$ state for each of the $X\,^3\Sigma_g^-$, $^1\Delta_g$, and $^1\Sigma_g^+$ electronic states of CO_2^{2+}, which we estimated using the spectroscopic constants reported in Ref. [116]. The upper limit is estimated by modeling our experimental conditions to determine when prompt breakup, i.e., events that do not significantly move in the spectrometer before dissociating, is separated from dissociation in flight. Note neither our data nor that of Long *et al.* [27] show any evidence of dissociation in flight of the $O_2^+ + C^+$ bond rearrangement channel.

On the other hand, a fraction of events of CO_2^{2+} breakup into $CO^+ + O^+$ are known to dissociate in flight [27,75], where Field and Eland reported a mean lifetime of 900 ns of the intermediate metastable CO_2^{2+} [75]. The angular distribution of the $CO^+ + O^+$ presented in Fig. 5 focuses on the prompt dissociation, which is observed to be aligned along the laser polarization, in contrast to the $O_2^+ + C^+$ bond rearrangement channel which is isotropic.

While the branching ratio for bond rearrangement processes in polyatomic molecules such as ammonia and methane [7] can vary over orders of magnitude (e.g., the large $H_2^+ + CH_2^+$ channel in methane), it is curious to note the relatively similar branching ratios for the triatomic molecules examined here. Despite the differences in the structure and bonding of

the molecules, and the observed differences in the angular distributions of the bond rearrangement fragments discussed above, the bond rearrangement branching ratios in double ionization are all within an order of magnitude of each other. This is consistent with previous measurements of similar branching ratios in water [30] and even acetylene [28], where the $H_2^+ + C_2^+$ channel was estimated to be 0.05% of the dominant ion-pair channel $H^+ + C_2H^+$. Theoretical treatment may reveal if the similarity in the branching ratios is just a coincidence or if there is a general predisposition for bond rearrangement involving two atoms located at the edges of a small molecule to occur at this level.

V. SUMMARY

The strong-field induced bond rearrangement branching ratio of three doubly ionized triatomic molecules (CO_2, OCS, and D_2O) was measured to provide comparative information about the bond rearrangement process in which the two edge atoms break from the center atom and reform into a diatomic ion. Out of these triatomic molecules, bond rearrangement occurs most often in water, which has an initially bent geometry and the least massive edge atoms. The mass-dependent trend extends to CO_2 and OCS, where the more massive sulfur atom on the edge of the OCS molecule can qualitatively explain the lower bond rearrangement branching ratio in OCS compared to CO_2.

Both D_2O and OCS are more likely to undergo bond rearrangement that ejects the newly formed molecular ion along the laser polarization, which is consistent with previous explanations of these processes [8,22,39,42]. Bond rearrangement in CO_2, in contrast, leads to a nearly isotropic distribution of the $O_2^+ + C^+$ breakup. Furthermore, OCS was the only molecule in which the bond rearrangement channel had an angular distribution that was similar to the main dissociative double ionization channel. Thus it appears that the details of the bond rearrangement mechanisms are different in the molecules studied here.

Despite these differences between CO_2, OCS, and D_2O, however, the double ionization bond rearrangement branching ratios are similar in the three molecules. This similarity is somewhat curious since the differences are much less than observed in similar measurements of slightly larger polyatomic molecules [7]. An increased theoretical understanding of these processes is necessary to determine if the similarities are a product of some general behavior of bond rearrangement in triatomic molecules.

[1] Y. Furukawa, K. Hoshina, K. Yamanouchi, and H. Nakano, Chem. Phys. Lett. **414**, 117 (2005).

[2] I. Ben-Itzhak, A. M. Sayler, M. Leonard, J. Maseberg, D. Hathiramani, E. Wells, M. Smith, J. Xia, P. Wang, K. Carnes, and B. Esry, Nucl. Instrum. Methods Phys. Res., Sect. B **233**, 284 (2005).

[3] T. Okino, Y. Furukawa, P. Liu, T. Ichikawa, R. Itakura, K. Hoshina, K. Yamanouchi, and H. Nakano, J. Phys. B **39**, S515 (2006).

[4] K. Hoshina, Y. Furukawa, T. Okino, and K. Yamanouchi, J. Chem. Phys. **129**, 104302 (2008).

[5] F. A. Rajgara, A. K. Dharmadhikari, D. Mathur, and C. P. Safvan, J. Chem. Phys. **130**, 231104 (2009).

[6] S. Kaziannis, I. Liontos, G. Karras, C. Corsi, M. Bellini, and C. Kosmidis, J. Chem. Phys. **131**, 144308 (2009).

[7] B. Jochim, A. Lueking, L. Doshier, S. Carey, E. Wells, E. Parke, M. Leonard, K. D. Carnes, and I. Ben-Itzhak, J. Phys. B **42**, 091002 (2009).

[8] J. Laksman, D. Céolin, M. Gisselbrecht, and S. L. Sorensen, J. Chem. Phys. **133**, 144314 (2010).

[9] K. Hoshina, H. Kawamura, M. Tsuge, M. Tamiya, and M. Ishiguro, J. Chem. Phys. **134**, 064324 (2011).

[10] P. M. Kraus, M. C. Schwarzer, N. Schirmel, G. Urbasch, G. Frenking, and K.-M. Weitzel, J. Chem. Phys. **134**, 114302 (2011).

[11] J. Laksman, E. P. Månsson, A. Sankari, D. Céolin, M. Gisselbrecht, and S. L. Sorensen, Phys. Chem. Chem. Phys. **15**, 19322 (2013).

[12] K. Nakai, T. Kato, H. Kono, and K. Yamanouchi, J. Chem. Phys. **139**, 181103 (2013).

[13] R. Fernando, A. Dey, B. M. Broderick, B. Fu, Z. Homayoon, J. M. Bowman, and A. G. Suits, J. Phys. Chem. A **119**, 7163 (2014).

[14] B. Wei, Y. Zhang, X. Wang, D. Lu, G. C. Lu, B. H. Zhang, Y. J. Tang, R. Hutton, and Y. Zou, J. Chem. Phys. **140**, 124303 (2014).

[15] H. Ibrahim, B. Wales, S. Beaulieu, B. E. Schmidt, N. Thiré, E. P. Fowe, É. Bisson, C. T. Hebeisen, V. Wanie, M. Giguére, J.-C. Kieffer, M. Spanner, A. D. Bandrauk, J. Sanderson, M. S. Schuurman, and F. Légaré, Nat. Commun. **5**, 4422 (2014).

[16] C. E. Liekhus-Schmaltz, I. Tenney, T. Osipov, A. Sanchez-Gonzalez, N. Berrah, R. Boll, C. Bomme, C. Bostedt, J. D. Bozek, S. Carron, R. Coffee, J. Devin, B. Erk, K. R. Ferguson, R. W. Field, L. Foucar, L. J. Frasinski, J. M. Glownia, M. Gühr, A. Kamalov, J. Krzywinski, H. Li, J. P. Marangos, T. J. Martinez, B. K. McFarland, S. Miyabe, B. Murphy, A. Natan, D. Rolles, A. Rudenko, M. Siano, E. R. Simpson, L. Spector, M. Swiggers, D. Walke, S. Wang, T. Weber, P. H. Bucksbaum, and V. S. Petrovic, Nat. Commun. **6**, 8199 (2015).

[17] S. Maeda, T. Taketsugu, K. Ohno, and K. Morokuma, J. Am. Chem. Soc. **137**, 3433 (2015).

[18] H. Wu, S. Zhang, J. Zhang, Y. Yang, L. Deng, T. Jia, Z. Wang, and Z. Sun, J. Phys. Chem. A **119**, 2052 (2015).

[19] P. L. Houston, R. Conte, and J. M. Bowman, J. Phys. Chem. A **120**, 5103 (2016).

[20] M. Kübel, R. Siemering, C. Burger, N. G. Kling, H. Li, A. S. Alnaser, B. Bergues, S. Zherebtsov, A. M. Azzeer, I. Ben-Itzhak, R. Moshammer, R. de Vivie-Riedle, and M. F. Kling, Phys. Rev. Lett. **116**, 193001 (2016).

[21] J. A. DeVine, M. L. Weichman, X. Zhou, J. Ma, B. Jiang, H. Guo, and D. M. Neumark, J. Am. Chem. Soc. **138**, 16417 (2016).

[22] D. Mathur, A. K. Dharmadhikari, J. A. Dharmadhikari, and P. Vasa, J. Phys. B **50**, 154004 (2017).

[23] P. Bhatt, T. Sairam, A. Kumar, H. Kumar, and C. P. Safvan, Phys. Rev. A **96**, 022710 (2017).

[24] N. Ekanayake, M. Nairat, B. Kaderiya, P. Feizollah, B. Jochim, T. Severt, B. Berry, K. R. Pandiri, K. D. Carnes, S. Pathak, D. Rolles, A. Rudenko, I. Ben-Itzhak, C. A. Mancuso, B. S. Fales, J. E. Jackson, B. G. Levine, and M. Dantus, Sci. Rep. **7**, 4703 (2017).

[25] J. A. DeVine, M. L. Weichman, B. Laws, J. Chang, M. C. Babin, G. Balerdi, C. Xie, C. L. Malbon, W. C. Lineberger, D. R. Yarkony, R. W. Field, S. T. Gibson, J. Ma, H. Guo, and D. M. Neumark, Science **358**, 336 (2017).

[26] S. Larimian, S. Erattupuzha, S. Mai, P. Marquetand, L. González, A. Baltuška, M. Kitzler, and X. Xie, Phys. Rev. A **95**, 011404(R) (2017).

[27] J. Long, F. J. Furch, J. Durá, A. S. Tremsin, J. Vallerga, C. P. Schulz, A. Rouzée, and M. J. J. Vrakking, J. Chem. Phys. **147**, 013919 (2017).

[28] S. Xu, H. Zhao, X. Zhu, D. Guo, W. Feng, K.-C. Lau, and X. Ma, Phys. Chem. Chem. Phys. **20**, 27725 (2018).

[29] N. Ekanayake, T. Severt, M. Nairat, N. P. Weingartz, B. M. Farris, B. Kaderiya, P. Feizollah, B. Jochim, F. Ziaee, K. Borne, K. Raju P., K. D. Carnes, D. Rolles, A. Rudenko, B. G. Levine, J. E. Jackson, I. Ben-Itzhak, and M. Dantus, Nat. Commun. **9**, 5186 (2018).

[30] M. Leonard, A. M. Sayler, K. D. Carnes, E. M. Kaufman, E. Wells, R. Cabrera-Trujillo, B. D. Esry, and I. Ben-Itzhak, Phys. Rev. A **99**, 012704 (2019).

[31] H. B. Gray, Nat. Chem. **1**, 7 (2009).

[32] M. P. Grubb, M. L. Warter, A. G. Suits, and S. W. North, J. Phys. Chem. Lett. **1**, 2455 (2010).

[33] M. P. Grubb, M. L. Warter, H. Xiao, S. Maeda, K. Morokuma, and S. W. North, Science **335**, 1075 (2012).

[34] Z. Lu, Y. C. Chang, Q.-Z. Yin, C. Y. Ng, and W. M. Jackson, Science **346**, 61 (2014).

[35] N. Schirmel, N. Reusch, P. Horsch, and K.-M. Weitzel, Faraday Discuss. **163**, 461 (2013).

[36] E. Wells, C. Rallis, M. Zohrabi, R. Siemering, B. Jochim, P. Andrews, U. Ablikim, B. Gaire, S. De, K. Carnes, B. Bergues, R. de Vivie-Riedle, M. Kling, and I. Ben-Itzhak, Nat. Commun. **4**, 2895 (2013).

[37] M. N. Piancastelli, A. Hempelmann, F. Heiser, O. Gessner, A. Rüdel, and U. Becker, Phys. Rev. A **59**, 300 (1999).

[38] A. Hiraya, K. Nobusada, M. Simon, K. Okada, T. Tokushima, Y. Senba, H. Yoshida, K. Kamimori, H. Okumura, Y. Shimizu, A.-L. Thomas, P. Millie, I. Koyano, and K. Ueda, Phys. Rev. A **63**, 042705 (2001).

[39] V. Brites, J. Eland, and M. Hochlaf, Chem. Phys. **346**, 23 (2008).

[40] J. Laksman, E. P. Månsson, C. Grunewald, A. Sankari, M. Gisselbrecht, D. Céolin, and S. L. Sorensen, J. Chem. Phys. **136**, 104303 (2012).

[41] J. H. D. Eland, S. Zagorodskikh, R. J. Squibb, M. Mucke, S. L. Sorensen, and R. Feifel, J. Chem. Phys. **140**, 184305 (2014).

[42] S. L. Sorensen, M. Gisselbrecht, J. Laksman, E. P. Månsson, D. Céolin, A. Sankari, and F. Afaneh, J. Phys.: Conf. Ser. **488**, 012006 (2014).

[43] M. Garg, A. K. Tiwari, and D. Mathur, J. Chem. Phys. **136**, 024320 (2012).

[44] H. C. Straub, B. G. Lindsay, K. A. Smith, and R. F. Stebbings, J. Chem. Phys. **108**, 109 (1998).

[45] B. Brehm, J. Eland, R. Frey, and H. Schulte, Int. J. Mass Spectrom. Ion Phys. **21**, 373 (1976).

[46] K. Wohrer, G. Sampoll, R. L. Watson, M. Chabot, O. Heber, and V. Horvat, Phys. Rev. A **46**, 3929 (1992).

[47] D. Mathur, Phys. Rep. **225**, 193 (1993).

[48] I. Ben-Itzhak, K. D. Carnes, S. G. Ginther, D. T. Johnson, P. J. Norris, and O. L. Weaver, Phys. Rev. A **47**, 3748 (1993).

[49] E. Wells, V. Krishnamurthi, K. D. Carnes, N. G. Johnson, H. D. Baxter, D. Moore, K. M. Bloom, B. M. Barnes, H. Tawara, and I. Ben-Itzhak, Phys. Rev. A **72**, 022726 (2005).

[50] J. Ullrich, R. Moshammer, R. Dörner, O. Jagutzki, V. Mergel, H. Schmidt-Böcking, and L. Spielberger, J. Phys. B **30**, 2917 (1997).

[51] J. Ullrich, R. Moshammer, A. Dorn, R. Dörner, L. P. H. Schmidt, and H. Schmidt-Böcking, Rep. Prog. Phys. **66**, 1463 (2003).

[52] G. A. McCracken, A. Kaldun, C. Liekhus-Schmaltz, and P. H. Bucksbaum, J. Chem. Phys. **147**, 124308 (2017).

[53] T. Shimanouchi, *Tables of Molecular Vibrational Frequencies Consolidated Volume I*, Vol. I (National Bureau of Standards, Gaithersburg, MD, 1972).

[54] X. Ren, A. M. Summers, K. Raju P., A. Vajdi, V. Makhija, C. W. Fehrenbach, N. G. Kling, K. J. Betsch, Z. Wang, M. F. Kling, K. D. Carnes, I. Ben-Itzhak, C. Trallero-Herrero, and V. Kumarappan, J. Opt. **19**, 124017 (2017).

[55] R. Trebino, K. W. DeLong, D. N. Fittinghoff, J. N. Sweetser, M. A. Krumbügel, B. A. Richman, and D. J. Kane, Rev. Sci. Instrum. **68**, 3277 (1997).

[56] V. L. B. de Jesus, B. Feuerstein, K. Zrost, D. Fischer, A. Rudenko, F. Afaneh, C. D. Schröter, R. Moshammer, and J. Ullrich, J. Phys. B **37**, L161 (2004).

[57] A. J. R. Heck and D. W. Chandler, Annu. Rev. Phys. Chem. **46**, 335 (1995).

[58] R. E. Continetti, Annu. Rev. Phys. Chem. **52**, 165 (2001).

[59] A. E. Slattery, T. A. Field, M. Ahmad, R. I. Hall, P. Lablanquie, and F. Penent, Meas. Sci. Technol. **13**, 2007 (2002).

[60] G. F. Knoll, *Radiation Detection and Measurement* (John Wiley and Sons Ltd., New York, 2010).

[61] X. Gong, Q. Song, Q. Ji, K. Lin, H. Pan, J. Ding, H. Zeng, and J. Wu, Phys. Rev. Lett. **114**, 163001 (2015).

[62] J. Eland, F. Wort, and R. Royds, J. Electron Spectrosc. Relat. Phenom. **41**, 297 (1986).

[63] I. Ben-Itzhak, S. Ginther, and K. Carnes, Nucl. Instrum. Methods Phys. Res., Sect. B **66**, 401 (1992).

[64] T. Jahnke, T. Weber, T. Osipov, A. Landers, O. Jagutzki, L. Schmidt, C. Cocke, M. Prior, H. Schmidt-Böcking, and R. Dörner, J. Electron Spectrosc. Relat. Phenom. **141**, 229 (2004), Frontiers of Coincidence Experiments.

[65] B. Gaire, A. M. Sayler, P. Q. Wang, N. G. Johnson, M. Leonard, E. Parke, K. D. Carnes, and I. Ben-Itzhak, Rev. Sci. Instrum. **78**, 024503 (2007).

[66] M. Berglund and M. E. Wieser, Pure Appl. Chem. **83**, 397 (2011).

[67] N. G. Kling, J. McKenna, A. M. Sayler, B. Gaire, M. Zohrabi, U. Ablikim, K. D. Carnes, and I. Ben-Itzhak, Phys. Rev. A **87**, 013418 (2013).

[68] W. Lai and C. Guo, Phys. Rev. A **92**, 013402 (2015).

[69] T. Masuoka, Phys. Rev. A **50**, 3886 (1994).

[70] G. Ohrwall, M. M. S. Anna, W. C. Stolte, I. Dominguez-Lopez, L. T. N. Dang, A. S. Schlachter, and D. W. Lindle, J. Phys. B **35**, 4543 (2002).

[71] Y. Muramatsu, K. Ueda, N. Saito, H. Chiba, M. Lavollée, A. Czasch, T. Weber, O. Jagutzki, H. Schmidt-Böcking, R. Moshammer, U. Becker, K. Kubozuka, and I. Koyano, Phys. Rev. Lett. **88**, 133002 (2002).

[72] Z. D. Pešić, D. Rolles, R. C. Bilodeau, I. Dimitriu, and N. Berrah, Phys. Rev. A **78**, 051401(R) (2008).

[73] R. K. Kushawaha, S. S. Kumar, I. A. Prajapati, K. P. Subramanian, and B. Bapat, J. Phys. B **42**, 105201 (2009).

[74] J. H. D. Eland, L. Andric, P. Linusson, L. Hedin, S. Plogmaker, J. Palaudoux, F. Penent, P. Lablanquie, and R. Feifel, J. Chem. Phys. **135**, 134309 (2011).

[75] T. A. Field and J. H. Eland, Chem. Phys. Lett. **211**, 436 (1993).

[76] A. E. Slattery, T. A. Field, M. Ahmad, R. I. Hall, J. Lambourne, F. Penent, P. Lablanquie, and J. H. D. Eland, J. Chem. Phys. **122**, 084317 (2005).

[77] V. Sharma, B. Bapat, J. Mondal, M. Hochlaf, K. Giri, and N. Sathyamurthy, J. Phys. Chem. A **111**, 10205 (2007).

[78] Y. Hikosaka, Y. Shibata, K. Soejima, H. Iwayama, and E. Shigemasa, Chem. Phys. Lett. **603**, 46 (2014).

[79] K. Ueda and J. H. D. Eland, J. Phys. B **38**, S839 (2005).

[80] C. Tian and C. R. Vidal, Phys. Rev. A **58**, 3783 (1998).

[81] B. Bapat and V. Sharma, J. Phys. B **40**, 13 (2006).

[82] X. Wang, Y. Zhang, D. Lu, G. C. Lu, B. Wei, B. H. Zhang, Y. J. Tang, R. Hutton, and Y. Zou, Phys. Rev. A **90**, 062705 (2014).

[83] E. Wang, X. Shan, Z. Shen, M. Gong, Y. Tang, Y. Pan, K.-C. Lau, and X. Chen, Phys. Rev. A **91**, 052711 (2015).

[84] N. Neumann, D. Hant, L. P. H. Schmidt, J. Titze, T. Jahnke, A. Czasch, M. S. Schöffler, K. Kreidi, O. Jagutzki, H. Schmidt-Böcking, and R. Dörner, Phys. Rev. Lett. **104**, 103201 (2010).

[85] M. R. Jana, P. N. Ghosh, B. Bapat, R. K. Kushawaha, K. Saha, I. A. Prajapati, and C. P. Safvan, Phys. Rev. A **84**, 062715 (2011).

[86] A. Khan, L. C. Tribedi, and D. Misra, Phys. Rev. A **92**, 030701(R) (2015).

[87] M. Alagia, P. Candori, S. Falcinelli, M. Lavollé, F. Pirani, R. Richter, S. Stranges, and F. Vecchiocattivi, J. Phys. Chem. A **113**, 14755 (2009).

[88] J. Eland, S. Plogmaker, P. Lablanquie, F. Penent, J. Palaudoux, C. Nicolas, E. Robert, C. Miron, and R. Feifel, Chem. Phys. Lett. **646**, 31 (2016).

[89] J. H. Sanderson, T. R. J. Goodworth, A. El-Zein, W. A. Bryan, W. R. Newell, A. J. Langley, and P. F. Taday, Phys. Rev. A **65**, 043403 (2002).

[90] W. A. Bryan, W. R. Newell, J. H. Sanderson, and A. J. Langley, Phys. Rev. A **74**, 053409 (2006).

[91] C. Wu, C. Wu, D. Song, H. Su, Y. Yang, Z. Wu, X. Liu, H. Liu, M. Li, Y. Deng, Y. Liu, L.-Y. Peng, H. Jiang, and Q. Gong, Phys. Rev. Lett. **110**, 103601 (2013).

[92] B. Wales, E. Bisson, R. Karimi, S. Beaulieu, A. Ramadhan, M. Giguére, Z. Long, W.-K. Liu, J.-C. Kieffer, F. Légaré, and J. Sanderson, J. Electron Spectrosc. Relat. Phenom. **195**, 332 (2014).

[93] J. Rajput, T. Severt, B. Berry, B. Jochim, P. Feizollah, B. Kaderiya, M. Zohrabi, U. Ablikim, F. Ziaee, K. Raju P., D. Rolles, A. Rudenko, K. D. Carnes, B. D. Esry, and I. Ben-Itzhak, Phys. Rev. Lett. **120**, 103001 (2018).

[94] T. Masuoka, I. Koyano, and N. Saito, J. Chem. Phys. **97**, 2392 (1992).

[95] T. Masuoka, J. Chem. Phys. **98**, 6989 (1993).

[96] R. Hall, L. Avaldi, G. Dawber, A. McConkey, M. MacDonald, and G. King, Chem. Phys. **187**, 125 (1994).

[97] K. Saha, S. Banerjee, and B. Bapat, Chem. Phys. Lett. **607**, 85 (2014).

[98] A. Ramadhan, B. Wales, R. Karimi, I. Gauthier, M. MacDonald, L. Zuin, and J. Sanderson, J. Phys. B **49**, 215602 (2016).

[99] B. Wales, T. Motojima, J. Matsumoto, Z. Long, W.-K. Liu, H. Shiromaru, and J. Sanderson, J. Phys. B **45**, 045205 (2012).

[100] H. Kumar, P. Bhatt, C. P. Safvan, and J. Rajput, J. Chem. Phys. **148**, 064302 (2018).

[101] Z. Shen, E. Wang, M. Gong, X. Shan, and X. Chen, J. Chem. Phys. **145**, 234303 (2016).

[102] A. M. Sayler, E. Wells, K. Carnes, and I. Ben-Itzhak, in *The CAARI 2000: Sixteenth International Conference on the Application of Accelerators in Research and Industry*, edited by I. L. Morgan, J. L. Duggan, and M. Hall, AIP Conf. Proc. No. 576 (AIP, Melville, NY, 2001), p. 33.

[103] A. M. Sayler, J. Maseberg, D. Hathiramani, K. Carnes, and I. Ben-Itzhak, in *Application of Accelerators in Research and Industry: 17th International Conference on the Application of Accelerators in Research and Industry* edited by J. L. Duggan, I. L. Morgan, and M. Hall, AIP Conf. Proc. No. 680 (AIP, Melville, NY, 2003), p. 48.

[104] P. Bunker, O. Bludsky, P. Jensen, S. Wesolowski, T. V. Huis, Y. Yamaguchi, and H. Schaefer, J. Mol. Spectrosc. **198**, 371 (1999).

[105] K. Codling and L. J. Frasinski, J. Phys. B **26**, 783 (1993).

[106] A. Rudenko, V. Makhija, A. Vajdi, T. Ergler, M. Schürholz, R. K. Kushawaha, J. Ullrich, R. Moshammer, and V. Kumarappan, Faraday Discuss. **194**, 463 (2016).

[107] T. Ando, A. Iwasaki, and K. Yamanouchi, Phys. Rev. Lett. **120**, 263002 (2018).

[108] L. Holmegaard, J. L. Hansen, L. Kalhøj, S. L. Kragh, H. Stapelfeldt, F. Filsinger, J. Küpper, G. Meijer, D. Dimitrovski, M. Abu-samha, C. P. J. Martiny, and L. B. Madsen, Nat. Phys. **6**, 428 (2010).

[109] J. L. Hansen, L. Holmegaard, J. H. Nielsen, H. Stapelfeldt, D. Dimitrovski, and L. B. Madsen, J. Phys. B **45**, 015101 (2011).

[110] R. Johansen, K. G. Bay, L. Christensen, J. Thøgersen, D. Dimitrovski, L. B. Madsen, and H. Stapelfeldt, J. Phys. B **49**, 205601 (2016).

[111] P. Sándor, A. Sissay, F. Mauger, P. M. Abanador, T. T. Gorman, T. D. Scarborough, M. B. Gaarde, K. Lopata, K. J. Schafer, and R. R. Jones, Phys. Rev. A **98**, 043425 (2018).

[112] J. Eland, Mol. Phys. **61**, 725 (1987).

[113] D. Pavičić, K. F. Lee, D. M. Rayner, P. B. Corkum, and D. M. Villeneuve, Phys. Rev. Lett. **98**, 243001 (2007).

[114] M. Oppermann, S. J. Weber, L. J. Frasinski, M. Y. Ivanov, and J. P. Marangos, Phys. Rev. A **88**, 043432 (2013).

[115] B. Jochim, R. Erdwien, Y. Malakar, T. Severt, B. Berry, P. Feizollah, J. Rajput, B. Kaderiya, W. L. Pearson, K. D. Carnes, A. Rudenko, and I. Ben-Itzhak, New J. Phys. **19**, 103006 (2017).

[116] M. Hochlaf, F. R. Bennett, G. Chambaud, and P. Rosmus, J. Phys. B **31**, 2163 (1998).